1 GENERAL

MAR-M-247 is a nickel-base casting alloy developed by the Martin-Marietta Corporation for applications requiring high strength at elevated temperatures up to about 1900F. Its balanced composition provides an excellent combination of tensile and creep-rupture properties as a result of gamma-prime strengthening enhanced by solid solution and grain-boundary strengthening. Evaluations after long-time exposures to normal operating temperatures – for example, creep-test specimens and turbine blades removed from service – reveal excellent microstructural and mechanical-property stability. This sluggish reaction to high-temperature exposures helps to maintain excellent notch toughness as well as high strength (Refs. 6, 20, 31, 40).

MAR-M-247 has good castability, which is an important characteristic for the production of critical gas-turbine components such as blades, discs, and integral wheel configurations. It is an outgrowth of MAR-M-246 with an addition of hafnium and adjustments in other alloy levels to optimize properties and castability (Ref. 6).

1.1 Commercial Designation
MAR-M-247

1.2 Alternate Designation
MM-0011 (Refs. 8,13)

1.3 Specifications

1.3.1 No AMS, ASTM, or other widely available specifications for MAR-M-247 had been published at the time of preparation of this document.

1.3.2 Some individual companies that use or produce the alloy, in all probability, have prepared their own proprietary specifications. AiResearch Corp., for example, developed company material specifications covering requirements for chemical composition, cleaning, and visual, penetrant, and x-ray inspections, etc.

1.4 Composition *[Table]*

	Ni
10.0	Co
10.0	W
8.25	Cr
5.5	Al
3.0	Ta
1.5	Hf
1.0	Ti
0.7	Mo
0.15	C
0.05	Zr
0.015	B

1.5 Heat Treatment

1.5.1 Although the combination of gamma-prime, solution, and grain-boundary strengthening are effective in the as-cast condition, heat-treatment – either aging alone (below 2000F) or solution (above 2000F) plus aging – is usually applied since it tends to improve properties (See Section 2.1.2.1)

1.5.1.1 Typical aging treatment alone consists of 1600F, 20 hr., AC. However, variations of this common treatment are also used, such as two-step aging consisting, for example, of 1800F five hr plus 1600F 20 hr, AC (Refs. 8, 16, 31, 42).

1.5.1.2 Typical solution-plus-aging treatment consists of 2250F two hr, argon quench, plus 1800F five hr plus 1600F 20hr, AC (Refs. 2, 16, 28, 41).

1.6 Hardness
Heat-treated: Rockwell C30-40 (Ref. 2)

1.7 Forms and Conditions Available
Available as conventional equiaxed investment castings and as directionally solidified castings. The material has also been produced in the form of single crystals; but for this type of casting, modified alloys with reduced contents of the grain boundary strengtheners (carbon, hafnium, boron, and zirconium) and some with additions of about three percent rhenium have gained wide acceptance (Refs. 11, 12, 14, 15, 16, 19, 20, 23, 24, 27, 30, 35, 36, 41).

1.8 Melting and Casting Practice
Generally, the alloy is induction melted and cast in vacuum. Conventional shell molds made by the lost-wax process are used for the production of equiaxed investment castings. Vacuum induction melting and casting and shell molds are also used in the production of directionally solidified and single-crystal products, but special processes and techniques are used to produce the temperature gradients and progressive solidification necessary to obtain the desired results. For this purpose, three different processes have been developed: the exothermic, withdrawal, and liquid-metal-cooling processes, all of which produce similar results (Refs. 14, 15, 23, 41).

1.9 Special Considerations

1.9.1 The mechanical properties of MAR-M-247 are markedly influenced by crystallographic orientation, which is quite significant in directionally solidi-

fied and single-crystal products, but not in conventional investment castings, which are equiaxed and isotropic. For example, loading of directionally solidified and single-crystal castings in the [111] orientation provides the best creep resistance.

However, loading in the [001] orientation, which coincides with the longitudinal orientation and the major stress axis in directionally solidified and single-crystal turbine blades, provides the best combination of properties; that is, good strength and creep-rupture life plus excellent thermal-fatigue resistance as a result of the relatively low Modulus of elasticity in that orientation (Refs. 2, 3, 4, 14, 23).

1.9.1.1 *[Figure]* Standard stereographic triangle showing relative stress-rupture lives at about 1400F of single crystals of MAR-M-247 as a function of crystallographic orientation with respect to the direction of loading.

1.9.2 Removal of cobalt from the alloy improves the cyclic oxidation resistance and hot corrosion resistance but adversely affects creep properties.

1.9.2.1 *[Table]* Effects of reducing cobalt content on various properties.

1.9.3 Grain size significantly influences the properties of MAR-M-247. Generally, finer grain size, produced by relatively rapid solidification, improves strength at low-to-intermediate temperatures up to about 1500F. For higher-temperature performance, coarser grains produced by slower solidification are preferred. For certain castings, the desired grain sizes are difficult to achieve. For example, for thin airfoils operating at the highest temperatures coarse grains would be desirable; whereas for the heavier-section root-attachment area, where service temperatures are lower, a fine-grain microstructure would be preferable. However, the normal solidification rates associated with these differences in section size tend to have the opposite effects on grain size. This type of problem can be mitigated to some degree by certain foundry techniques, such as creating deliberate hot spots in the mold to retard the solidification rates in selected areas.

The Howmet Corp. has developed two grain-refining processes in conjunction with hot-isostatic-pressing (HIP): Grainex and Microcast-X, which can provide ASTM grain sizes as fine as two (Grainex) and three to five (Microcast-X), respectively (Refs. 23, 40 p. 992)

1.9.4 Hot-isostatic-pressing (HIP), which involves the simultaneous application of heat and pressure, can be used to virtually eliminate internal porosity from MAR-M-247 castings, thereby improving mechanical properties. In this process, argon is normally applied at pressures of 15 to 30 ksi at temperatures of 2200 to 2225F. Some products, however, for example MAR-M-247 heavy-section castings such as integral wheels, have been found to undergo incipient melting when hot-isostatically-pressed at 2200F and 15 ksi for four hours. To prevent this type of damage and still eliminate porosity, the HIP parameters were modified to 2165F and 25 ksi for four hours. This type of trade-off between temperature and pressure can also be used to prevent grain growth and to inhibit carbide degradation (Refs. 23, 40 pp. 993-4).

2 PHYSICAL PROPERTIES AND ENVIRONMENTAL EFFECTS

2.1 Thermal Properties

2.1.1 Melting Range: 2400 to 2450F (Ref. 42)

2.1.2 Phase Changes and Time-Temperature-Transformation Diagrams

2.1.2.1 MAR-M-247 consists of about 60 percent coherent gamma-prime phase, Ni_3 (Al, Ti), in a matrix of gamma, which is a nickel-rich solid solution strengthened by alloy additions of cobalt, molybdenum, tungsten, chromium, and tantalum. The gamma-prime phase is the main strengthening component. Carbon, boron, zirconium, and hafnium, mostly in the form of carbides and borides, precipitate at the grain boundaries and contribute to strength and ductility. In addition, elemental segregation during solidification causes the formation of small amounts of a gamma/gamma-prime eutectic and carbides interspersed in the interdendritic areas. Heat treatment mitigates segregation, refines the gamma-prime dispersion in the gamma matrix, eliminates some of the gamma/gamma-prime eutectic, and optimizes the grain-boundary carbide morphology and distribution, most of which benefit mechanical properties.

The alloy exhibits excellent microstructural stability at normal operating temperatures. It is resistant to the precipitation of unwanted intermetallics and of carbides of undesirable morphology. A study of the effects of high-temperature service was conducted on investment-cast gas-turbine blades that had been in service at 1400-1545F for 548 hours plus 146 heat-up/cool-down cycles (Ref. 31). The service exposures induced some precipitation of small secondary gamma-prime particles and agglomeration of the primary gamma-prime particles. Nevertheless, tensile and creep-rupture tests at 1560 and 1650F and high-cycle fatigue tests at 1560F on specimens from both the used blades and similar unused blades showed that the minor microstructural changes had little effect on mechanical properties (Refs. 6, 14, 20, 28, 31, 39)

2.1.2.1.1 *[Figure]* Larson-Miller plot comparing stress-rupture properties of used and unused gas-turbine blades.
Note: Generally, this Handbook prefers to present creep and rupture properties in terms of direct test data rather than in terms of a time-temperature relationship such as the Larson-Miller parameter. In this particular instance, as well in Figures 3.4.9 and 3.4.11, Larson-Miller plots are used because direct test data were not available. Whereas these plots can be useful for comparative purposes, they should be used with great caution when extrapolation outside the data range is attempted.
(See Section 3.4 in the section "General Discussion of Handbook Contents" in Volume 1 of this Handbook.)

2.1.3 Thermal Conductivity

2.1.3.1 *[Figure]* Thermal conductivity of directionally solidified alloy.

2.1.4 Thermal Expansion

2.1.4.1 *[Figure]* Thermal expansion of MAR-M-247 in two different forms and conditions.

2.1.5 Specific Heat

2.1.6 Thermal Diffusivity

2.2 Other Physical Properties

2.2.1 Density: 0.308 lb. in^{-3}, 8.54 gm cc^{-3} (Refs. 16, 35, 36, 42).

2.2.2 Electrical Properties

2.2.3 Magnetic Properties

2.2.4 Emittance

2.2.5 Damping Capacity

2.3 Chemical Environments

2.3.1 General Corrosion

2.3.1.1 Protective coatings are required for MAR-M-247, as well as other superalloys, to protect against oxidation and hot corrosion (sulfidation) in high-temperature applications such as turbine engines. Generally, either: aluminide diffusion coatings (RT-21) or MCrAl overlay coatings applied by plasma spray or vapor deposition are used for such applications. (M=Metal, for example nickel, cobalt or a combination). Under conditions of cyclic stress-strain and excess coating thickness (greater than 0.002 in.) cracks may initiate in aluminide diffusion coatings and propagate into the base metal. In one series of tests at 1600F, a tin aluminide diffusion coating, 0.001-0.002 in. thick had no detrimental effects on the fatigue life of MAR-M-247 up to at least 10^7 cycles (Ref. 41, pp. 132-5). For the MCrAl overlay coatings, greater thickness can be applied without deleterious effects; however, disadvantages compared with aluminide coatings are the inability to coat internal channels, the need for increased apparatus, and the inability to coat large batches (Refs. 38, 41, 43, 44).

2.3.1.1.1 *[Figure]* Oxidation resistance in air at 2012F of MAR-M-247 and of two alloy variations with reduced cobalt content.

2.3.1.1.2 *[Figure]* Results of tests at 1700F on bare and aluminide (RT-21) coated alloy in the AiResearch oxidation, hot-corrosion burner rig.

2.3.1.1.3 *[Figure]* Effects of variations in specimen temperature, gas velocity, and sodium chloride content of gas on surface deterioration due to seven hours of impingement by combustion gases from lamp oil containing 0.5 percent sulfur. The sodium chloride was derived from the injection of an aqueous salt solution into the combustion chamber.

2.3.2 Stress Corrosion

2.4 Nuclear Environments

3 MECHANICAL PROPERTIES

3.1 Specified mechanical Properties

3.1.1 Minimum room-temperature tensile properties specified for directionally solidified alloy by acceptance standard in Reference 2:

Ftu = 140 ksi
Fty = 120 ksi
e(4D) = 7.0%
RA = 7.0%

3.2 Mechanical Properties at Room Temperature See Section 3.3

3.2.1 Tension Stress-Strain Diagrams and Tensile Properties

3.2.1.1 *[Figure]* Weibull plot showing comparison of tensile strength of the alloy with IN-100 for specimens machined from integrally cast turbine wheels.

3.2.1.2 *[Figure]* Weibull plot showing comparison of 0.2 percent yield strength of the alloy with IN-100 for specimens machined from integrally cast turbine wheels.

3.2.1.3 *[Figure]* Weibull plot showing comparison of elongation of the alloy with IN-100 for specimens machined form integrally cast turbine wheels.

3.2.2 Compression Stress-Strain Diagrams and Compression Properties

3.2.3 Impact

3.2.4 Bending

3.2.5 Torsion and Shear

3.2.6 Bearing

3.4.13 *[Figure]* Effects of cobalt content on creep-rupture life and steady-state creep rate at 1400F and 1800F.

3.4.14 *[Figure]* Creep-rupture life at 1900F and 19 ksi of specimens machined in the longitudinal orientation [001] from single crystals of MAR-M-247 and five modified alloys intended for possible single-crystal applications.

3.5 Fatigue Properties

3.5.1 Conventional High-Cycle Fatigue

3.5.1.1 *[Table]* Fatigue strength (axial loading) at 10^7 cycles of conventional investment-cast blade/disc rotors at several temperatures and A ratios.

3.5.1.2 *[Table]* Fatigue strength (axial loading, longitudinal [001] orientation) at 10^7 cycles of directionally solidified test bars at 1600F.

3.5.1.3 *[Figure]* Load-controlled high-cycle fatigue test results for directionally solidified alloy, smooth and notched specimens, and longitudinal [001] orientation, at room temperature.

3.5.1.4 *[Figure]* Load-controlled high-cycle axial fatigue test results for directionally solidified alloy, smooth and notched specimens, and longitudinal [001] orientation, at 1600F.

3.5.1.5 *[Figure]* Estimated endurance limits at 10^7 cycles from load-controlled axial fatigue tests, longitudinal [001] specimen orientation.

3.5.2 Low Cycle Fatigue

3.5.2.1 *[Figure]* Effect of grain orientation of the directionally solidified alloy on thermal-fatigue life of coated and uncoated notched specimens.

3.5.2.2 *[Figure]* Low-cycle fatigue life as a function of total cyclic strain (excluding thermal expansion and contraction) with coordinated strain and temperature cycling.

3.5.2.3 *[Figure]* Low-cycle fatigue life as a function of total cyclic strain at two temperatures and two strain rates.

3.5.2.4 *[Figure]* Low-cycle fatigue life at three elevated temperatures as a function of total cyclic strain for investment-cast, grain-refined, HIP'd alloy.

3.5.2.5 *[Figure]* Low-cycle fatigue life under load control at 1400F for smooth coated and uncoated specimens from directionally solidified test bars.

3.5.2.6 *[Figure]* Low-cycle fatigue life under load control at 1400F for notched uncoated specimens from directionally solidified test bars.

3.5.3 Fatigue Crack Propagation

3.6 Elastic Properties

3.6.1 Poisson's Ratio

3.6.2 Modulus of Elasticity

3.6.2.1 In general, the modulus of elasticity of single-crystal and directionally solidified nickel and nickel-base superalloys varies widely with specimen orientation with respect to the crystal lattice, minimum modulus in the [001] direction and maximum in the [111] direction. Whereas Figure 3.3.1.12 shows the limited available test data on the effects of orientation on the elastic modulus of MAR-M-247, the following test results on NASAIR 100 (a derivative alloy for single crystals) and on pure nickel are probably reasonable approximations of the minimum and maximum modulus levels of MAR-M-247, corresponding to the [001] and [111] orientations respectively:

NASAIR-100, 75F, [001] – 16.6×10^6 psi

Nickel, 75F, [001] – 18.2×10^6 psi

NASAIR-100, 75F, [111] – 40.7×10^6 psi

Nickel, 75F, [111] – 42.6×10^6 psi

NASAIR-100, 1800F, [001] – 12.1×10^6 psi

NASAIR-100, 1800F, [111] – 31.2×10^6 psi

The deviation of the NASAIR-100 chemistry from that of MAR-M-247 consists primarily of the elimination of practically all of the cobalt and the grain-boundary strengtheners (carbon, hafnium, boron, and zirconium) from the composition (Refs. 41 p. 88, 147-149).

3.6.2.2 In Figure 3.6.2.2.1, the relatively low modulus values of MAR-M-247 are reasonably consistent with the longitudinal [001] grain orientation of the specimens.

3.6.2.2.1 *[Figure]* Modulus of elasticity in longitudinal [001] grain orientation for test specimens machined form directionally solidified alloy.

3.6.2.3 The following modulus of elasticity values were determined from the recorded stress-strain relationships in strain-controlled low-cycle fatigue tests on conventional investment-cast MAR-M-247, grain refined, HIP'd, solution treated at 2165F two hours and aged at 1600F 20 hours:

400F – 30.4×10^6 psi
800F – 29.4×10^6 psi
1400F – 25.3×10^6 psi

Each value is a average of eight test results. Since the tests were conducted on equiaxed alloy, they should represent a reasonable integration of the modulus-of-elasticity values for all of the crystallographic orientation (Ref 25).

3.6.2.3.1 *[Figure]* Range of modulus of elasticity values determined by numerous tests on eqiaxed castings at temperature form 75 to 2000F.

3.6.3 Modulus of Rigidity

3.6.3.1 *[Figure]* Range of modulus of rigidity values determined by numerous tests on equiaxed casings at temperatures from 75 to 2000F.

3.6.4 Tangent Modulus

3.6.5 Secant Modulus

4 FABRICATION

4.1 Forming

4.2 Machining and Grinding

4.3 Joining

4.3.1 MAR-M-247 is one of the most difficult alloys to bond by conventional fusion welding. However, Transient Liquid Phase (TLP) bonding has been applied successfully to the alloy. This technique uses modified MAR-M-247 filler metal containing relatively large amounts of boron (greater than two percent) and fabricated into flexible foils by rapid solidification processes. The bonding process is carried out under controlled bonding pressure in vacuum furnaces similar to those used for brazing. The filler metal temporarily melts and then resolidifies at the bonding temperature (approximately 2200F) in correlation with boron diffusion into the base metal. With proper control of the joining parameters and subsequent age hardening, the microstructure and tensile strength of TLP joints approach those of the base metal; for creep-rupture properties, maximum joint efficiencies of about 75 percent have been attained (Ref. 26, 33).

4.3.2 MAR-M-247 has also been joined by Solid-State-Diffusion bonding, which is quite similar to TLP (discussed in the preceding paragraph) except that no filler metal is used. One study evaluated the following process variables: temperature, surface toughness, and bonding pressure and time. The results showed joint tensile strength equal to that of the base metal but inconsistent and unsatisfactory creep-rupture properties (Ref. 21).

4.4 Surface Treating

References

1. International Nickel Company, Inc., "High Temperature, High Strength Nickel Base Alloy" (July, 1997).
2. Sink, L. W., Hoppin, G. S. III, and Fujii, M., "Low Cost Directionally-Solidified Turbine Blades", NASA CR-159464, AiResearch 21-2953 (January, 1979) pp 243-247.
3. Bizon, P. T., Dreshfield, R. L., and Calfo, F. D., "Effect of Grain Orientation and Casting on Thermal Fatigue Resistance of a Directionally-Solidified Superalloy MAR-M-247" NASA TM-79129 (April, 1979).
4. MacKay, A. R., Dreshfield , R. L., and Maier, R. D., "Anisotropy of Nickel-Base Superalloy Single Crystals", *Metallurgical Transactions*, Vol 13A (October, 1982).
5. Harris, K., Schwer, R. E., "Vacuum Induction Refined MM0011 (MAR-M-247) For Investment Cast Turbine Components", Sixth International Vacuum Metallurgy Conference, International Conference on Special Melting, San Diego, California, Cannon-Muskegan Corp., Muskegan, Michigan (April 23-27, 1979).
6. Martin-Marietta Corporation, Special Communication to MCIC (1979).
7. NASA Third Annual 'MATE' Review (March 29, 1979).
8. Harris, K., and Schwer, R. E., "Vacuum Induction Refining MM0011 (MAR-M-247) For High Integrity Turbine Rotating Parts", TMS-AIME Fall Meeting in St. Louis (October, 1978).
9. Nathal, M. V., Maier, R. D., and Ebert, L. J., "The Influence of Cobalt on the Tensile and Stress-Rupture Properties of the Nickel-Base Superalloy MAR-M-247", *Metallurigical Transactions*, Vol 13A (1982), pp. 1767-1774.
10. Stephens, J. R., "A Status Review of NASA's COSAM (Conservation of Strategic Aerospace Materials) Program", NASA TM-82852 (May, 1982).
11. Broomfield, R. W., Ford, D. A., Bhangu, H.K., Thomas, M. C., Frasier, D. J., Burkholder, P. S., Harris, K., Erickson, G. L., and Wahl, J. B., "Development and Turbine Engine Performance of Three Advanced Rhenium Containing Superalloys for Single Crystal and Directionally Solidified Blades and Vanes", Presented at the International Gas Turbine and Aeroengine Congress and Exhibition, Orlando, Florida (June, 1997).
12. McColvin, G. M., Sutton, J., Whitehurst, M., Fleck, D. G., VanVranken, T. A., Harris, K., Erickson, G. L., and Wahl, J. B., "Application of the Second Generation DS Superalloy CM-186-LC to First Stage Turbine Blading in EGT Industrial Gas Turbines", Presented at the Institute of Materials, Fourth International Charles Parsons Turbine Conference, Newcastle Upon Tyne, UK (November, 1997).

13. Martin-Marietta Corporation, Patents 3,677,747 and 3,720,509.

14. MacKay, A. R., and Maier, R. D., "Orientation Dependence of the Stress-Rupture Properties of Nickel-Base Superalloy Single Crystals" Case Western Reserve University, NASA CR-165394 (May, 1981).

15. Nathal , M. V., and Ebert, L. J., "Influence of Composition on the Microstructure and Mechanical Properties of Nickel-Base Superalloy Single Crystal", NASA Technical Memorandum 83563 (October, 1984).

16. Harris, K., Erickson, G. L., and Schwer, R. E., "MAR-M Derivations–CM247 LC DS Alloy, CMSX Single Crystal Alloys, Properties and Performance", Proceedings of the Fifth International Symposium on Superalloys, Metallurgical Society of AIME (October, 1984).

17. Tien, J. K., and Jarett, R. N., "Effects of Cobalt in Nickel-Base Superalloys", Columbia University, NASA CR-168308 (October, 1982).

18. Barrett, C. A., "The Effect of Variations of Cobalt Content on the Cyclic Oxidation Resistance of Selected Nickel-Base Superalloys", Lewis Research Center, NASA Technical Memorandum 87297 (March, 1986).

19. Strangeman, T. E., Dennis, R. E., and Heath, B. R., "Low-Cost, Single-Crystal Turbine Blades", Volume 2, Garrett Turbine Engine Co., NASA CR-174652 (April, 1984).

20. Nugyen, H. C., "The Effect of Tantalum and Carbon on the Structure, Properties of a Single-Crystal Nickel-Base Superalloy", Michigan Technological University, NASA CR-174779 (October, 1984).

21. Haufler, G., Mayer, H. G., Klatt, H., and Schreck, K., "Diffusion Bonding of Cast and EB-Welding of PM Nickel-Base Superalloys", Paper Presented at Conference on High-Temperature Alloys for Gas Turbines and Other Applications, Liege Belgium (October, 1986).

22. Ishida, A., Tomizuka, I., Ogawa, K., Sato, Y., and Yamazaki, M., "Effects of Environmental Factors on Hot Corrosion of a Nickel-Base Superalloy MM-247 in Flowing Combustion Gases", Transactions of National Research Institute for Metals (Japan), Vol. 30, No.1 (1988).

23. Dardi, L. E., Dalal, R. P., And Yaker, C., "Metallurgical Advancements in Investment Casting Technology" Proceedings of the Nicholas J. Grant Symposium, Processing and Properties of Advanced High-Temperature Alloys, MIT (June, 1985).

24. Harris, K., Erickson, G. L., Sikkenga, S. L., Brentnall, J. M., Aurrecoechea, J. M., and Kubarych, K. G., "Development of the Rhenium Containing Superalloys CMSX-4 and CM-186-LC for Single Crystal Blade and Directionally Solidified Vane Applications in Advanced Turbine Engines", Presented at the Seventh International Symposium on Superalloys, Seven Springs (September 1992).

25. Kaufman, M., "Properties of Cast MAR-M-247 for Turbine Blisk Applications", Proceedings of the Fifth International Symposium on Superalloys, Metallurgical Society AIME (October, 1984).

26. Nakahashi, M., Suenaga, S., Shirokave, M., and Takeda, H., "Transient Liquid Phase Bonding for Ni-Base Superalloys, MAR-M-247 and IN939", Materials Transactions, JIM (January, 1992).

27. MacKay, R. A., Nathal, M. V., "Microstructure-Property Relationships in Directionally Solidified Single Crystal Nickel-Base Superalloys", Lewis Research Center, NASA Technical Memorandum 88788.

28. Boismier, D.A., and Sehitogla, H., "Thermo-Mechanical Fatigue of MAR-M-247: Part 1-Experiments", Transactions AIME, Vol. 112 (January 1990)

29. Sehitogla, H., and Boismier, D.A., "Thermo-Mechanical Fatigue of MAR-M-247: Part 2-Life Prediction", Transactions AIME, Vol. 112 (January 1990)

30. DeLuca, D. P., and Hatala, R. W., "Single Crystal PWA1472 in High Pressure Hydrogen", Included in *Superalloys 718, 625, and 706 and Various Deviations*, The Minerals, Metals and Materials Society (1994).

31. Ohta, Y., Yoshizawa, H., and Nakagawa, Y. G., "Microstructural Changes in a Nickel-Base Superalloy During Service", Scripta Metallurgica, Vol. 23, pp 1609-1614 (1989).

32. Kuhn, H.A., and Sockel, H. G., "Elastic Properties of Textured and Directionally Solidified Nickel-Based Superalloys Between 25 and 1200C", Materials Science and Engineering, A112, pp. 117-126 (1989).

33. Nakagawa, Y. G., Yoshizawa, H., and Terashima, H., "Superplastic MAR-M-247 LC Superalloy Made by Compaction of Rapidly Solidified Ribbons", Materials Science and Technology, Vol. 2 (June, 1986).

34. "Materials for Advanced Turbine Engine (MATE) Program", Quarterly Progress Report No. 72 prepared by Garrett Turbine Engine Co. for NASA-Lewis Research Center (February 12, 1982).

35. Harris, K., Erickson, G. L., and Schwer, R. E., "CMSX Single Crystal, CM DS and Integral Wheel Alloys Properties and Performance", Presented at the Cost/501 Conference, Liege Belgium (October, 1986).

36. Harris, K., Erickson, G. L., and Schwer, R. E., "Development of a High Creep Strength, High Ductility, Cast Superalloy for Integral Turbine Wheels-CM MAR-M-247-LC", Presented at AIME Annual Meeting (February 1982).

37. Erickson, G. L., Harris, K., and Schwer, R. E., "Directionally Solidified DS CM-247 LC–Optimized

Mechanical Properties Resulting from Extensive Gamma Prime Solutioning", Presented at the Gas Turbine Conference and Exhibit, Houston, Texas (March 1985).

38. Korinko, P. S., Barber, M. J., and Thomas, M., "Coating Characterization and Evaluation of Directionally Solidified CM-186-LC and Single Crystal CMSX-4", Presented at the ASME Turbo Expo '96, Birmingham, UK (June 1996).

39. Nathal, M. V., and Ebert, L. J., "Gamma Prime Shape Changes During Creep of a Nickel-Based Superalloy", Scripta Metallurgica, Vol. 17, pp. 1151-1154 (1983).

40. Metals Handbook, ASM International, Tenth Edition, Vol. 1, pp. 981-994 (1990).

41. Strangeman, T. E., Heath, B., and Fujii, "Low-Cost Single-Crystal Turbine Blades", Vol. 1, Garrett Turbine Engine Co., NASA CR-168218 (November, 1983).

42. Nickel Development Institute (courtesy of Inco Limited), "High -Temperature High Strength Nickel-Base Alloys", No. 393 (May 1995).

43. Pilsner, B. H., " Effects of MAR-M-247 Substrate (modified) Composition on Coating Oxidation and Coating/ Substrate Interdiffusion", Michigan Technological University, NASA CR-174851 (February 1985).

44. Burkholder, P. S., Thomas, M. C., Frasier, D. J., Whetstone, J. R., Harris, K., Erickson, G. L., Sikkenga, S. L., and Eridon, J. M., "Allison Engine Testing CMSX-4 Single Crystal Turbine Blades and Vanes", Presented at the Institute of Materials Third International Charles Parsons Turbine Conference, Newcastle Upon Tyne, UK (April 1995).

Table 1.4 Composition (Refs. 2, 41)

Alloy		MAR-M-147	
		Weight Percent	
Composition	Min	Max	Suggested Aim
Co	9.0	11.0	010.0
W	9.5	10.5	10.0
Al	5.3	5.7	5.5
Ta	2.8	3.3	3.0
Hf	1.2	1.6	1.5
Ti	0.9	1.2	1.0
Mo	0.5	0.8	0.7
C	0.13	0.17	0.15
Zr	0.03	0.08	0.05
B	0.01	0.02	0.015
Mg	—	0.20	–
S	–	0.015	–
Si	–	0.20	–
Fe	–	0.50	–
Ni	Remainder		

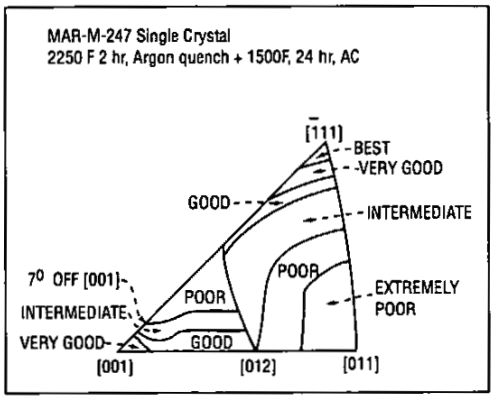

Figure 1.9.1.1 Standard sterographic traingle showing relative stress-rupture lives at about 1400F of single crystals of MAR-M-247 as a function of crystallographic orientation with respect to the direction of loading (Ref. 14)

Table 1.9.2.1 Effects of reducing cobalt content on various properties (Refs. 9, 10, 17, 18)

Alloy: MAR-M-247	
Form: Investment Cast	
Condition: Aged	
Property	Effect
Tensile	Minimal Effect
Creep-Rupture Life (See Figure 3.4.12 & 3.4.13)	50% reduction-decrease total removal-decrease
Creep Rate (See Figure 3.4.12 & 3.4.13)	50% reduction-increase total removal-increase
Oxidation Resistance	Improves (See Figure 2.3.1.1.1)
Corrosion Resistance	Improves
Long-term Stability	Improves
Contributing Factors γ' Volume fraction and particle size Carbide monphology and composition Stacking fault energy γ-γ' Mismatch	

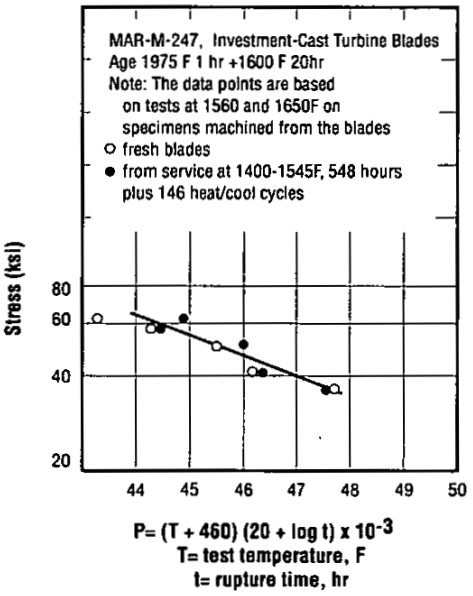

Figure 2.1.2.1.1 Larson-Miller plot comparing stress-rupture properties of used and unused gas-turbine blades (Ref. 31)

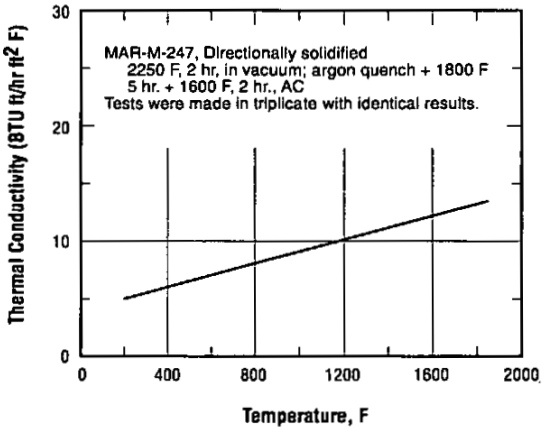

Figure 2.1.3.1 Thermal conducitivity of directionally solidified alloy (Ref. 2)

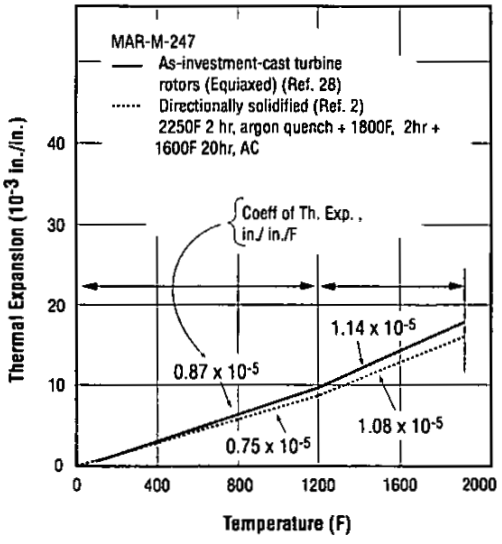

Figure 2.1.4.1 Thermal expansion of MAR-M-247 in two different forms and conditions (Refs. 2, 28)

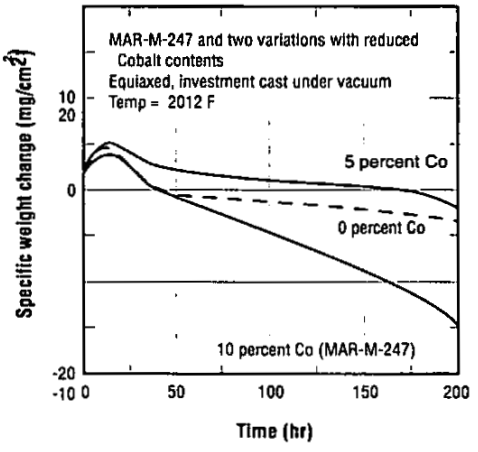

Figure 2.3.1.1.1 Oxidation resistance in air at 2012 F of MAR-M-247 and of two alloy variations with reduced colbalt contents (Ref. 10)

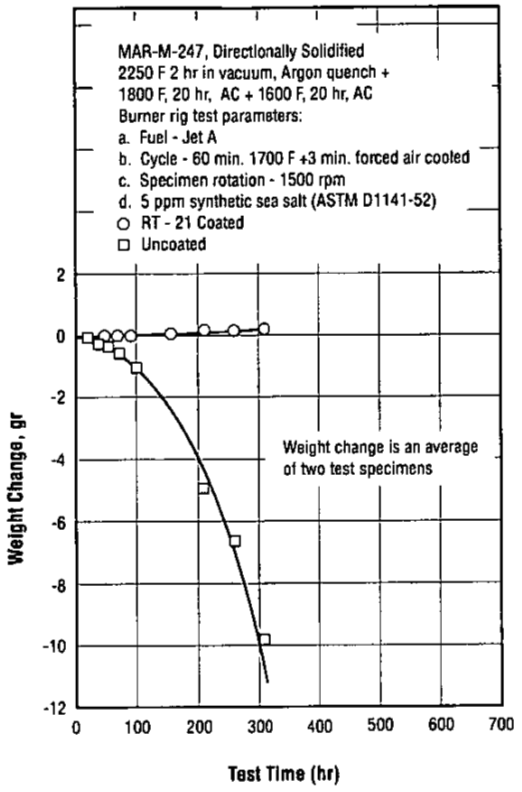

Figure 2.3.1.1.2 Results of tests at 1700 F on bare and aluminide (RT-21) coated alloy in AiResearch oxidation, hot-corrosion burner rig (Refs. 2, 41)

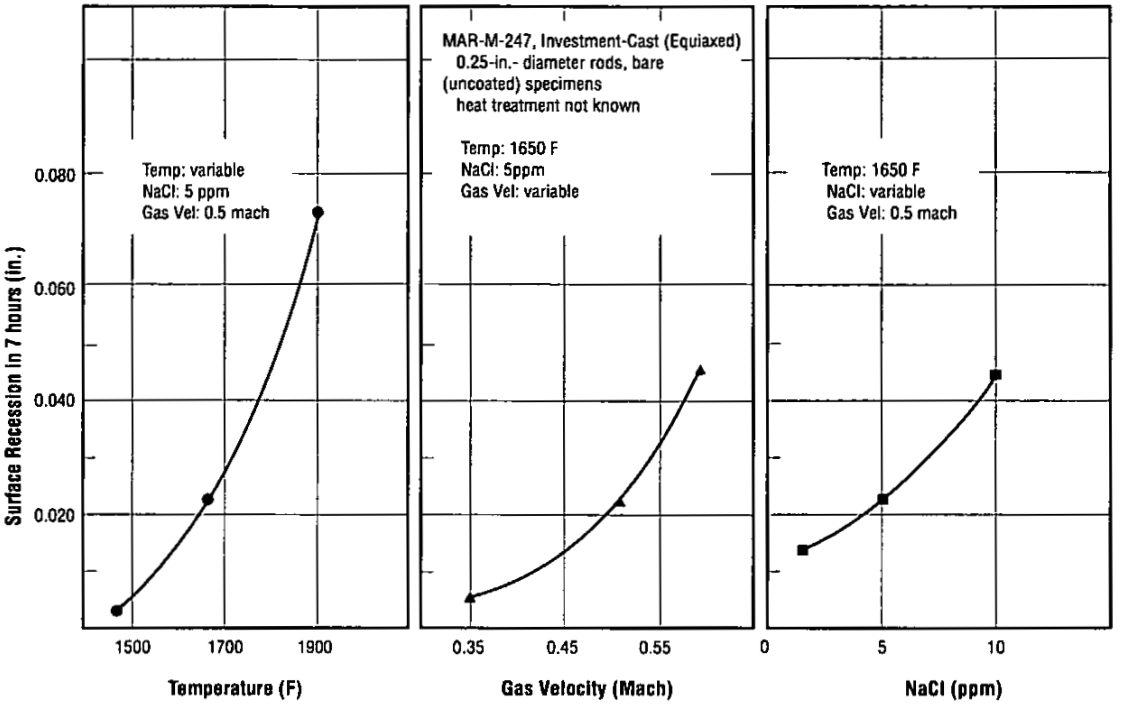

Figure 2.3.1.1.3 Effects of variations in specimen temperature, gas velocity, and sodium-chloride content of gas on surface deterioration due to seven hours of impingement by combustion gases from lamp oil containing 0.5 percent sulfur. The sodium-chloride was derived from the injection of an aqueous salt solution into the combustion chamber (Ref. 22)

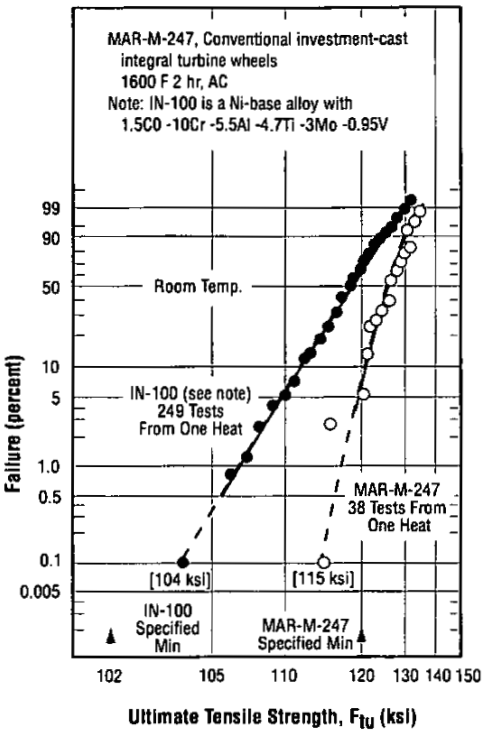

Figure 3.2.1.1 Weibull plot showing comparison of tensile strength of the alloy with IN-100 for specimens machined from intergrally cast turbine wheels (Ref. 5)

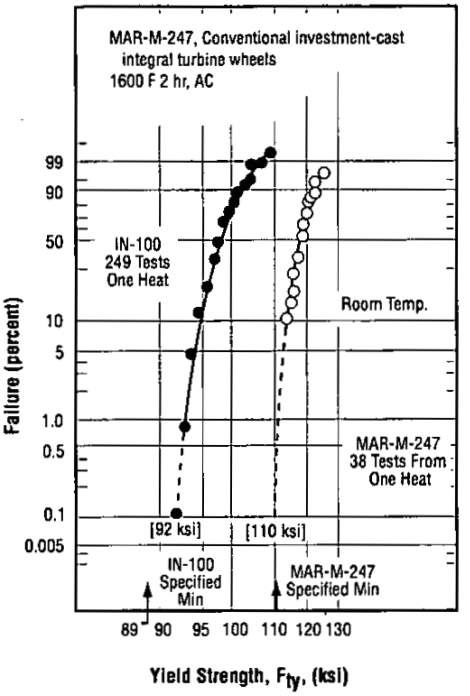

Figure 3.2.1.2 Weibull plot showing comparison of 0.2 percent yield strength of the alloy with IN-100 for specimens machined from integrally cast turbine wheels (Ref. 5)

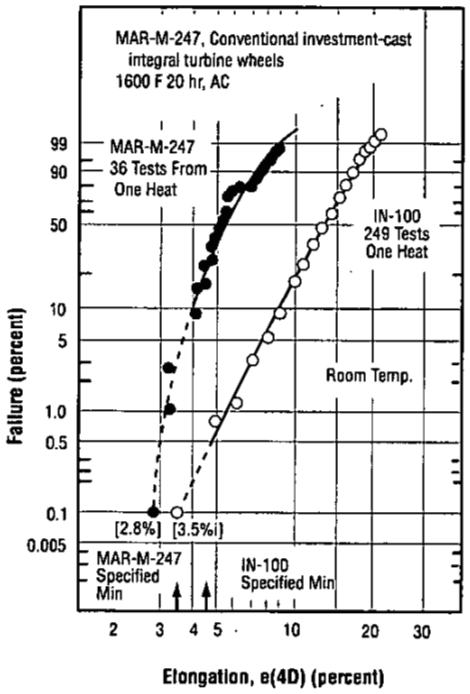

Figure 3.2.1.3 Weibull plot showing comparison of elongation of the alloy with IN-100 for specimens machined from intergrally cast turbine wheels (Ref. 5)

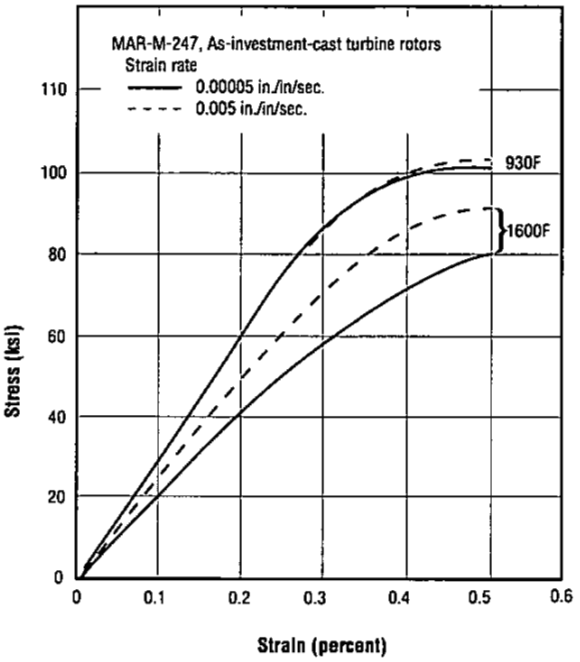

Figure 3.3.1.1 Tensile stress-strain curves at elevated temperatures and two different strain rates (Ref. 28)

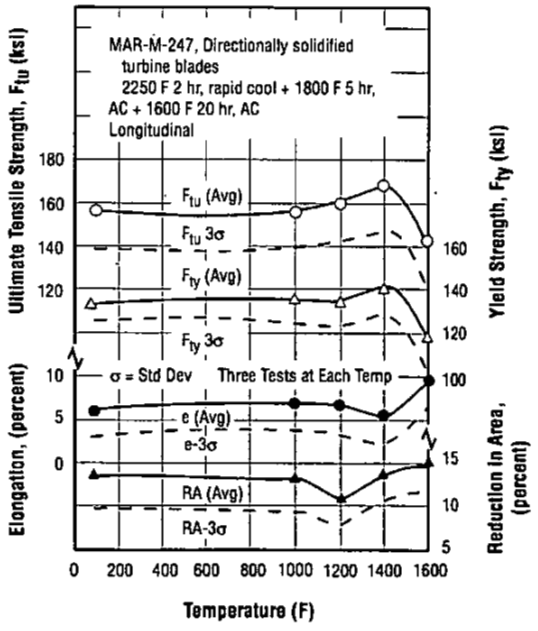

Figure 3.3.1.2 Effects of elevated temperatures on the longitudinal tensile properties of directionally solidified turbine blades (Ref. 2)

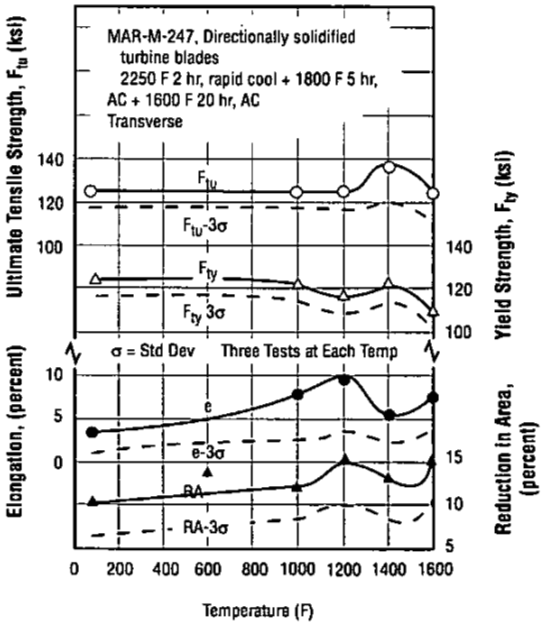

Figure 3.3.1.3 Effects of elevated temperatures on the transverse tensile properties of directionally solidified turbine blades (Ref. 2)

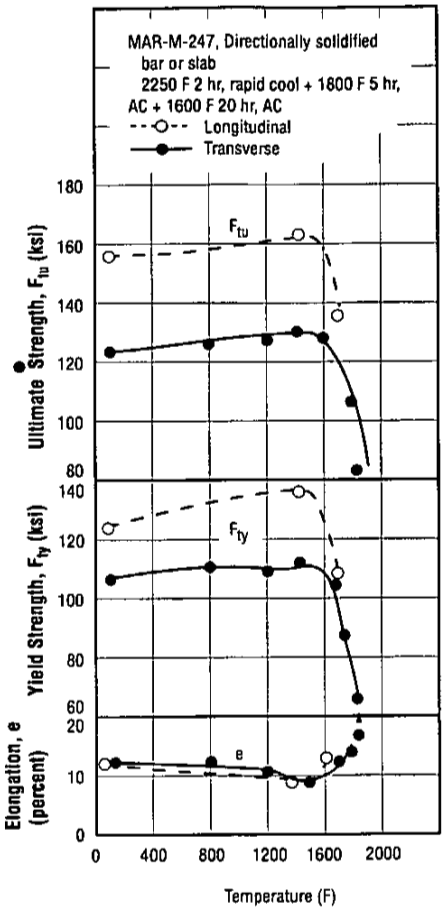

Figure 3.3.1.4 Effects of elevated temperatures on the longitudinal and transverse tensile properties of directionally solidified bar or slab (Ref. 37)

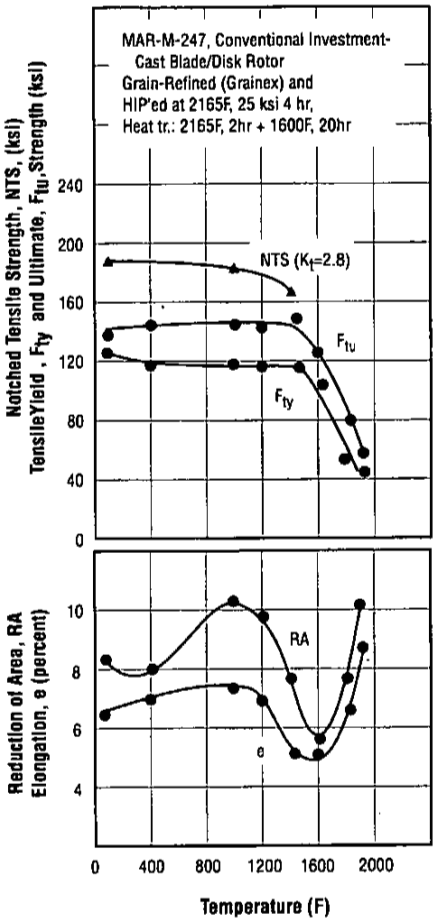

Figure 3.3.1.5 Effects of elevated temperatures on the tensile and notched-tensile properties of investment-cast, grain-refined, HIP'ed blade/disc rotor (Ref. 37)

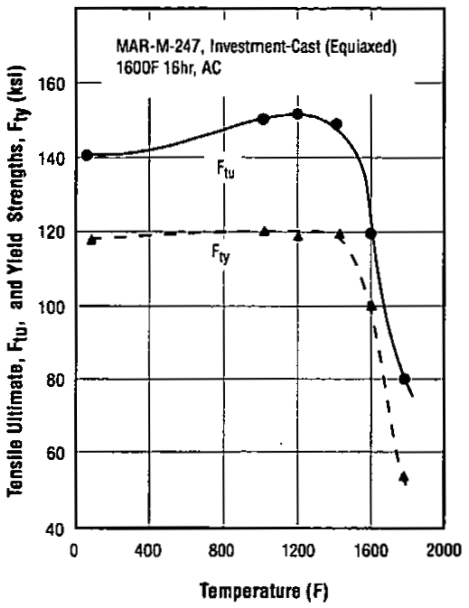

Figure 3.3.1.6 Tensile-strength properties of conventional investment castings at temperatures up to 1800F (Ref. 42)

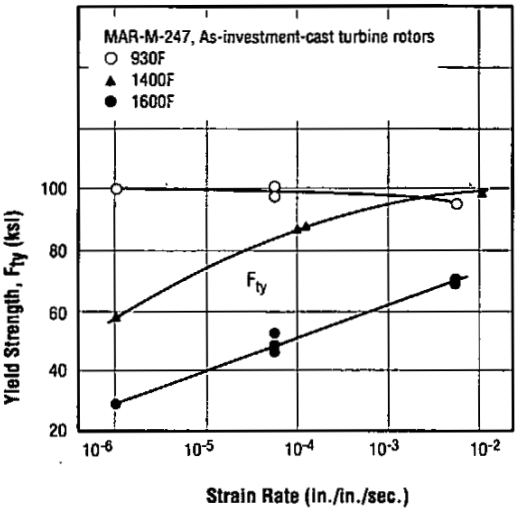

Figure 3.3.1.7 Effects of strain rate on tensile yield strength (F_{ty}) at several elevated temperatures (Ref. 29)

Table 3.3.1.8 Tensile properties of conventional investment-cast integral wheel at 70F and 800F (Ref. 36)

Alloy	MAR-M-247			
Form	Investment-Cast Integral Wheel (Equiaxed)			
Condition	1600F 2 hr, AC			
Temperature (F)	F_{ty} (ksi)	F_{tu} (ksi)	e (percent)	RA (percent)
70	118	123	4.8	9.5
800	117	128	4.6	8.1

Table 3.3.1.9 Elevated-temperature tensile properties of directionally solidified alloy in longitudinal [001] orientation (Ref. 16)

Alloy	MAR-M-247			
Form	Directionally Solidified			
Condition	1600F 2 hr, AC			
Temperature (F)	F_{ty} (ksi)	F_{tu} (ksi)	e (percent)	RA (percent)
1200	108.2	124.3	6.4	8.1
1380	118.0	136.0	5.5	6.5
1560	121.6	125.4	6.9	6.0

Table 3.3.1.10 Tensile properties of single-crystal and directionally solidified turbine blades in longitudinal and transverse orientations at 75F and 1400F (Ref. 41)

Alloy	MAR-M-247					
Form	Turbine Blades					
Condition	2275F 2 hr. + 1800F 5 hr. + 1600F 20 hr.					
Temperature (F)	Crystals	Orientation	F_{ty} (ksi)	F_{tu} (ksi)	e (percent)	RA (percent)
75	Single	Long	134	140	11.2	–
75	Dir. Solid	Long	132	154	5.8	–
75	Single	Transverse	123	133	11.1	19.2
75	Dir. Solid	Transverse	124	127	–	–
1400	Single	Long	135	151	6.7	–
1400	Dir. Solid	Long	140	168	6.0	–
1400	Single	Transverse	124	144	9.7	16.3
1400	Dir. Solid	Transverse	121	136	6.0	–

Table 3.3.1.11 Tensile properties of single-crystal ingots in transverse orientation at 75F and 1400F (Ref. 41)

Alloy	MAR-M-247			
Form	Single-Crystal Ingot			
Condition	2275F 2 hr. + 1800F 5 hr. + 1600F 20 hr.			
Temperature (F)	F_{ty} (ksi)	F_{tu} (ksi)	e (percent)	RA (percent)
75	124	132	9.8	22.0
1400	122	137	10.6	17.8

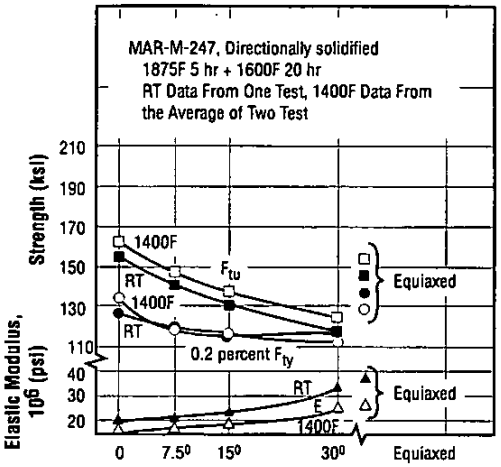

Figure 3.3.1.12 Effects of test specimen orientation with respect to the growth axis [001] of directional solidification on tensile ultimate and yield strengths and elastic modulus at room temperature and 1400F. Comparable properties of equiaxed specimens are also shown. (Ref. 3)

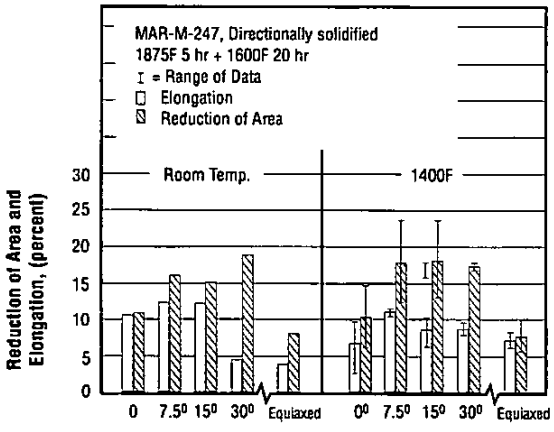

Figure 3.3.1.13 Effects of test specimen orientation with respect to the growth axis [001] of directional solidification on tensile elongation and reduction of area (Ref. 3)

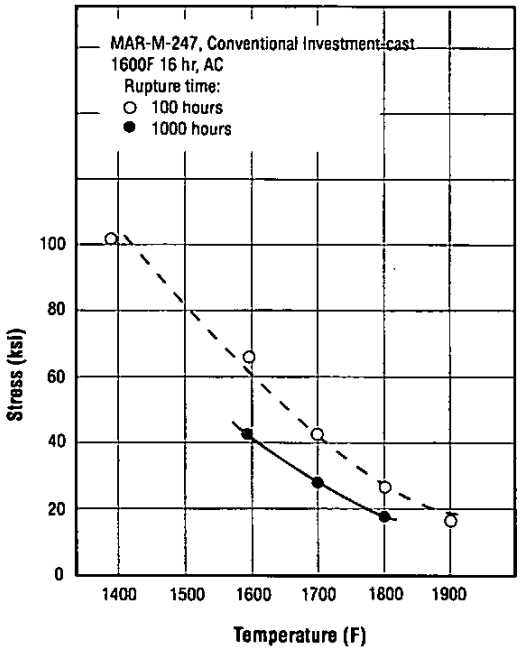

Figure 3.4.1. Effect of increasing temperatures on the stress to cause creep rupture of equiaxed turbine blades in 100 and 1000 hours (Refs. 1, 42)

Table 3.4.2 Creep-rupture properties of conventional equiaxed investment-cast blade/disc rotors at several temperatures and stress levels (Ref. 25)

Alloy		MAR-M-247					
Form		Conventional Investment-Cast Blade/Disc Rotor, Grain-Refined (Grainex) and HIP'ed at 2165F, 25 ksi, 4 hr.					
Condition		2165F 2hr + 1600F 20 hr					
Temperature (F)	Stress (ksi)	Creep Time (hr) to				Elong.	RA
		0.5%	1.0%	2.0%	Rupture	(percent)	
1400	90	250	–	–	274.7	1.1	1.1
1400	90	125	–	–	140.9	1.0	1.9
1400	90	183	–	–	300.2	1.5	3.4
1600	55	42	77	124	217.9	7.6	8.1
1600	45	309	451	628	818	5.9	7.5
1600	45	203	336	–	724.6	6.1	7.8
1800	25	57	88	114	126.6	5.4	5.3
1800	22	224	287	348	412.1	5.9	8.9
1800	22	139	178	214	220.8	4.0	5.3

Table 3.4.3 Creep-rupture properties of conventional investment-cast integral wheels at 1400F and 1800F (Refs. 36, p 17)

Alloy		MAR-M-247		
Form		Investment-Cast Integral Wheels (Equiaxed)		
Condition		1600F 20hr, AC		
Temperature (F)	Stress (ksi)	Rupture Tine (hr)	Elong. (percent)	RA (percent)
1400	97.5	131.3	5.0	12.4
1800	32.0	57.1	6.6	5.5

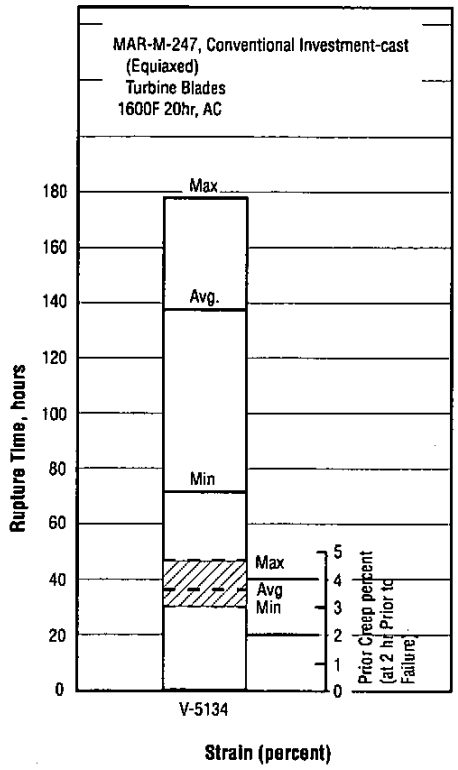

Figure 3.4.4 Creep-rupture time and prior creep (elongation at 2 hours prior to rupture) of the alloy tested at 100.7 ksi and 1400F (Ref. 8)

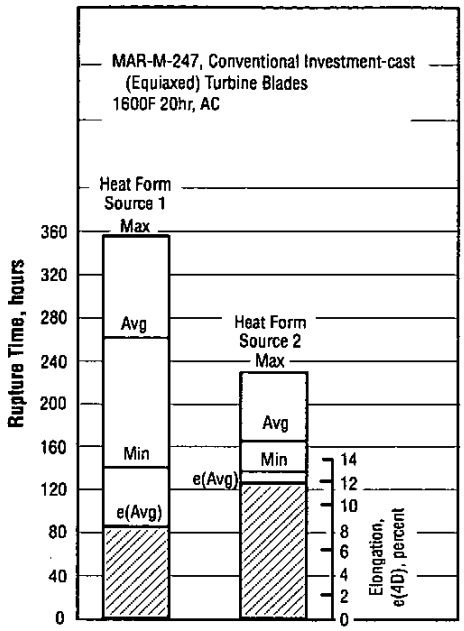

Figure 3.4.5 Comparison of creep-rupture time and total creep elongation of two different heats of the alloy at 15.66 ksi and 1900F (Ref. 8)

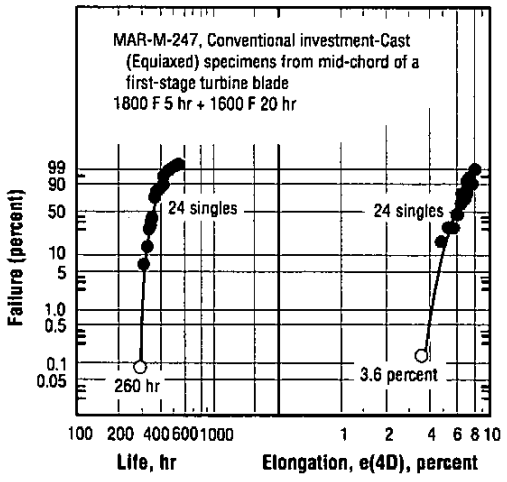

Figure 3.4.6 Weibull probability plot of creep-rupture data from tests conducted at 40 ksi and 1650 F on equiaxed specimens (Ref. 8)

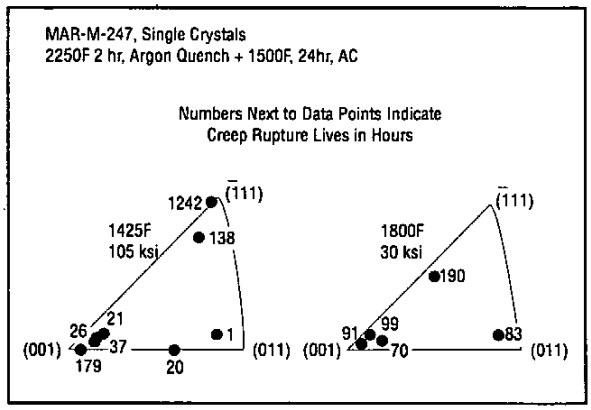

Figure 3.4.7 Effects of crystallographic orientation of loading direction on creep-rupture life of single crystals (Refs. 4, 14)

Table 3.4.8 Creep-rupture properties of single-crystal turbine blades in the longitudinal [001] and transverse orientations at three test temperatures after solution treatment at two different temperatures (Ref. 41, pp. 37, 38)

Alloy		MAR-M-247				
Form		Single Crystal Turbine Blades				
Condition		Solution-treated as indicated 2 hr., argon quench, 1800F 5 hr. + 1600F 20 hr.				
Temperature (F)		Specimen Orientation	Stress (ksi)	Rupture Time(hr)	Elongation	RA
Solution	Test				(percent)	
2250	1800	Long	30	126.4	17.2	43.6
2275	1800	Long	30	113.4	20.3	46.7
2275	1800	Transverse	30	102.8	25.1	41.2
2275	1800	Transverse	27	181.3	17.1	46.4
2250	1800	Transverse	27	148.8	17.8	37.6
2250	1900	Long	19	168.1	21.4	52.1
2275	1900	Long	19	206.8	20.0	57.3
2250	1900	Transverse	19	119.6	16.6	36.6
2275	1900	Transverse	19	172.2	19.9	45.5
2275	2000	Long	15	48.3	17.5	40.2
2275	2000	Transverse	14	78.5	20.6	40.1

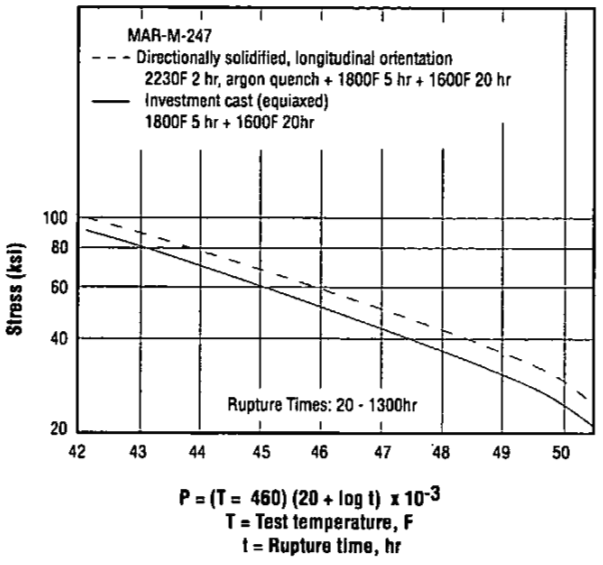

Figure 3.4.9 Larson-Miller parameter plot comparing stress-rupture properties of conventional investment cast alloy with directionally solidified alloy (Refs. 16, 36 p. 22, 40 p. 998)

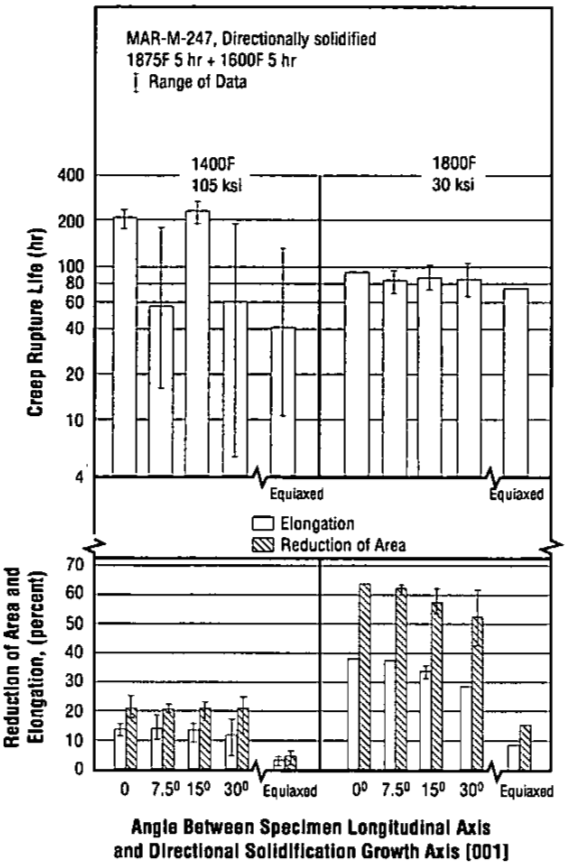

Figure 3.4.10 Effects of directional-solidification grain orientation on creep-rupture properties of the alloy, and comparison with equiaxed alloy at 1400F and 1800F (Ref. 3)

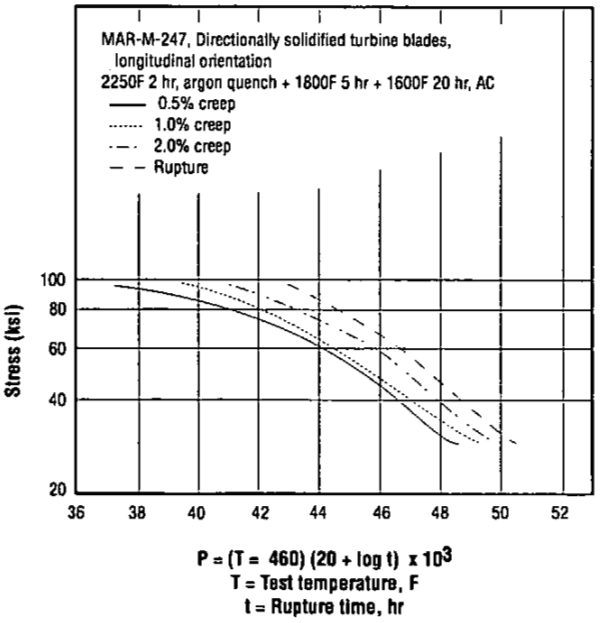

Figure 3.4.11 Larson-Miller parameter plot for various amounts of creep strain and rupture of directionally solidified alloy (Ref. 2)

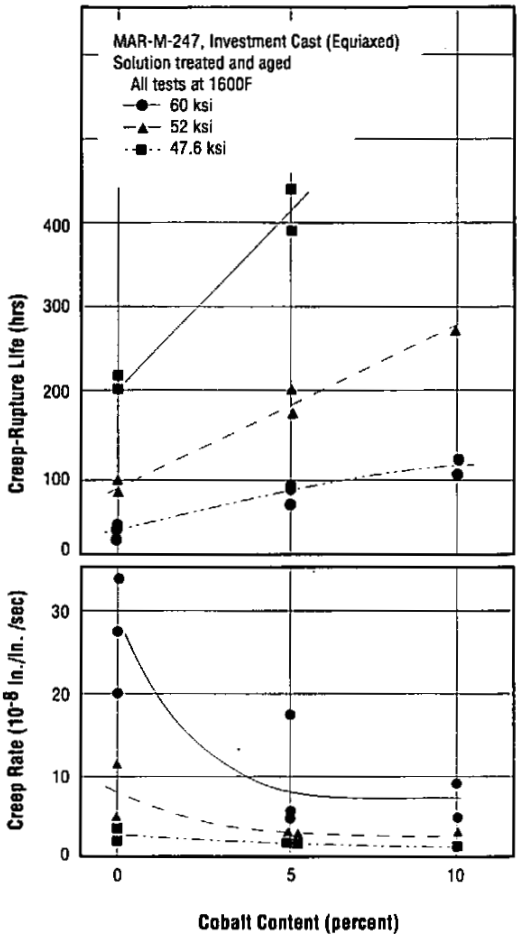

Figure 3.4.12 Effects of cobalt content on creep-rupture life and steady-state creep rate at 1600F (Ref. 9)

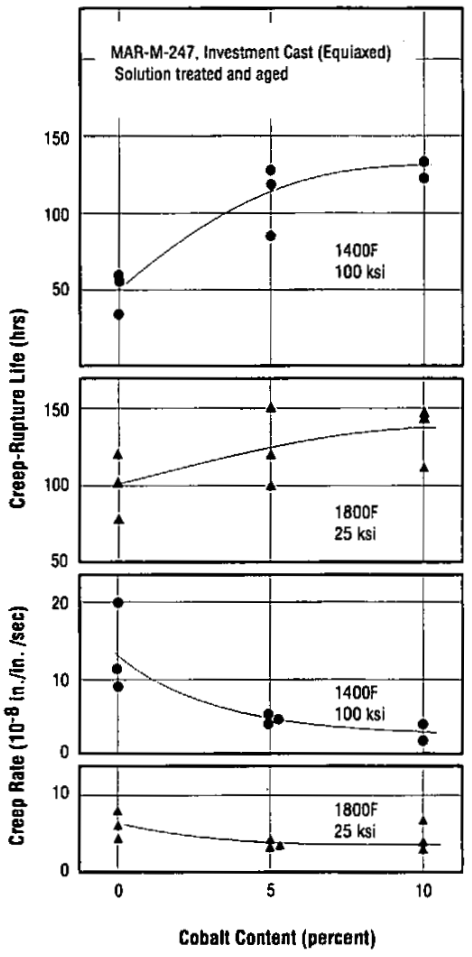

Figure 3.4.13 Effects of cobalt content on creep-rupture life and steady-state creep rate at 1400F and 1800F (Ref. 9)

MAR-M-247
Plus 5 modified compositions
for possible single-crystal applications.
Turbine blades-single crystal
Heat treatment not known
Note: The relatively high content of
zirconium in the modified alloys are
probably a result of the use of zirconia
melting crucibles.

Elements (percent)	MAR-M-247	Modified Alloys				
	Range	1	2	3	4	5
Mo	0.50 - 0.80	0.86	0.88	0.89	1.90	.83
W	9.50 - 10.50	10.51	10.40	10.2	10.48	10.62
Ta	2.80 - 3.80	3.61	3.61	3.29	3.54	3.69
Ti	0.90 - 1.20	1.14	0.97	0.95	0.98	1.15
Cr	8.00 - 8.80	8.99	8.20	8.58	8.06	8.38
Co	9.00 - 11.00	–	–	5.45	–	–
Al	5.30 - 5.70	5.44	5.39	5.34	5.40	5.45
C	0.13 - 0.17	0.016	0.009	0.007	0.008	0.016
Hf	1.20 -1.60	–	0.59	0.57	–	–
Zr	0.03 - 0.08	0.27	0.28	0.24	0.46	0.14
Y	–	–	–	–	–	0.04
Ni	Bal	Bal	Bal	Bal	Bal	Bal

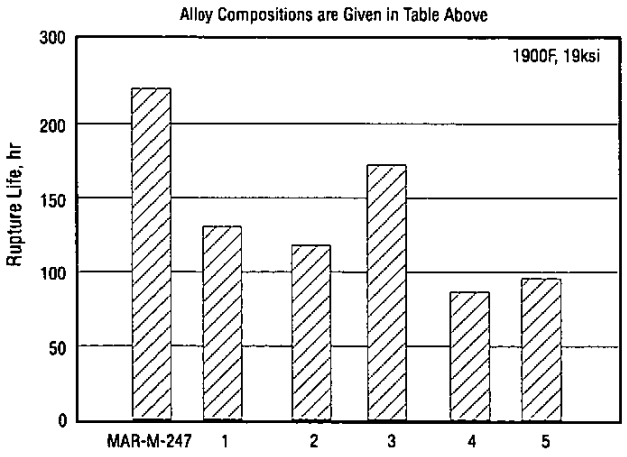

Figure 3.4.14 Creep-rupture life at 1900F and 19ksi of specimens machined in the longitudinal orientation [001] from single crystals of MAR-M-247 and five modified alloys intended for possible single-crystal application (Ref. 7)

Table 3.5.1.1 Fatigue strength (axial loading) at 10^7 cycles of conventional (equiaxed) investment-cast blade/disc rotors at several temperatures and A ratios (Ref. 25)

Alloy	MAR-M-247	
Form	Conventional Investment-Cast Blade/Disc Rotor, Grain Refined (Grainex) and HIP"ed at 2165F, 25 ksi, 4 hr.	
Condition	2165F 2 hr. + 1600F 20 hr.	
Test Temperature (F)	A Ratio	Fatigue Strength at 10^7 Cycles (ksi)
1100	∞	32.5
	0.67	29.2
	0.25	22.1
1500	∞	45.0
	0.25	18.8
1700	∞	36.6
	0.67	25.0
	0.25	13.7

Note: $A\ Ratio = \frac{alternating\ stress}{mean\ stress}$

$alternating\ stress = \frac{max.\ stress - min.\ stress}{2}$

Table 3.5.1.2 Fatigue strength (axial loading, longitudinal [001] orientation) at 10^7 cycles of directionally solidified test bars at 1600F (Ref. 34)

Alloy	MAR-M-247		
Form	Directionally Solidified Test Bars		
Condition	Solution Treated and Aged		
Temperature (F)	Surface Coating	A Ratio	Fatigue Strength at 10^7 Cycles (ksi)
1600	Uncoated	∞	38
	RT-21 Aluminide	∞	38
	Uncoated	0.95	55

Note: $A\ Ratio = \frac{alternating\ stress}{mean\ stress}$

$alternating\ stress = \frac{max.\ stress - min.\ stress}{2}$

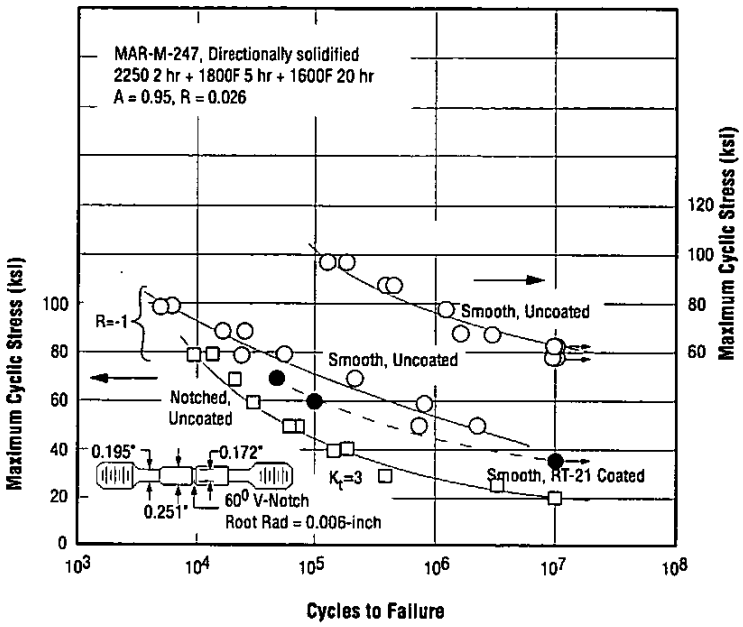

Figure 3.5.1.3 Load-controlled high-cycle axial fatigue test results for directionally solidified alloy, smooth and notched specimens, logitudinal [001] orientiation, at room temperature (Ref. 2)

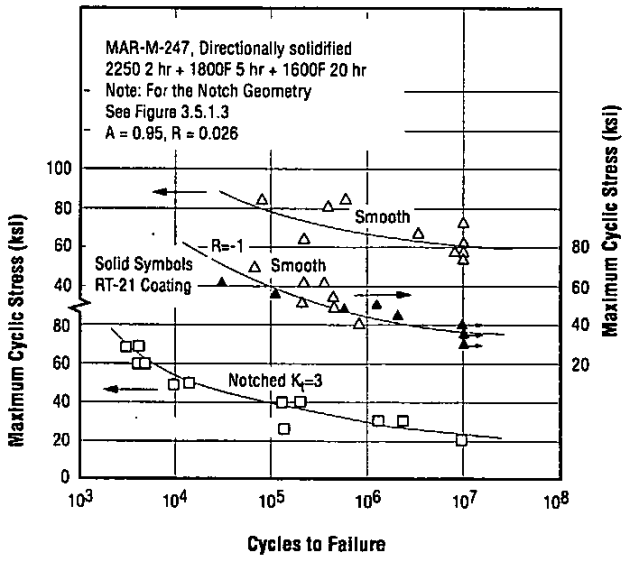

Figure 3.5.1.4 Load-controlled high-cycle axial-fatigue test results for directionally solidified alloy, smooth and notched specimens, logitudinal [001]orientiation, at 1600F (Ref. 2)

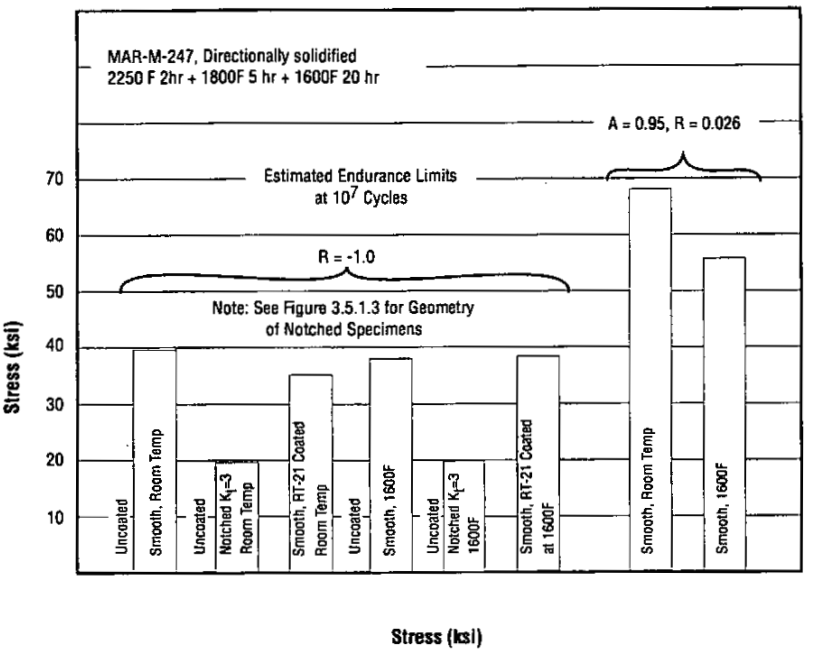

Figure 3.5.1.5 Estimated endurance limits at 10^7 cycles from load-controlled axial fatigue tests, longitudinal [001] specimen orientation (Ref. 2)

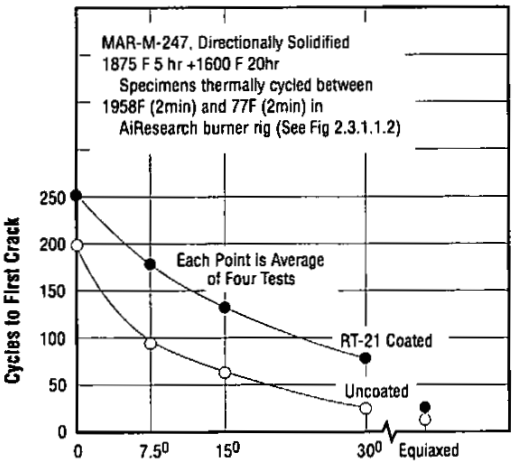

Figure 3.5.2.1 Effects of grain orientation of the directionally solidified alloy on the thermal-fatigue life of coated and uncoated notched specimens (Ref. 3)

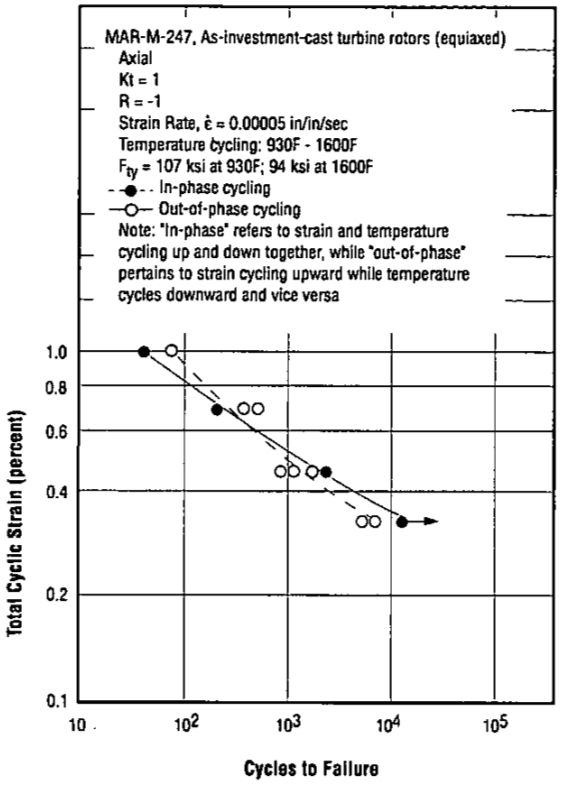

Figure 3.5.2.2 Low-cycle fatigue life as a function of total cyclic strain (excluding thermal expansion and contraction) with coordinated strain and temperature cycling (Refs. 28, 29)

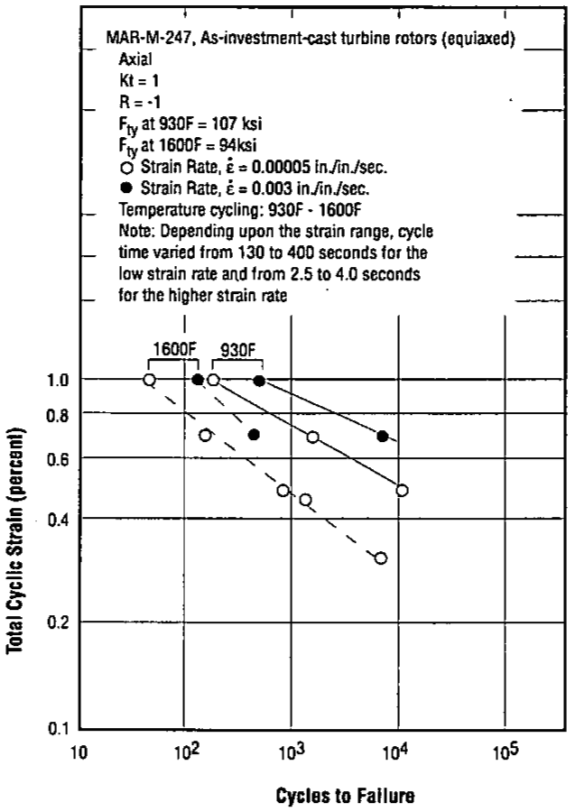

Figure 3.5.2.3 Low-cycle fatigue life as a function of total cyclic strain at two temperatures and two strain rates (Refs. 28, 29)

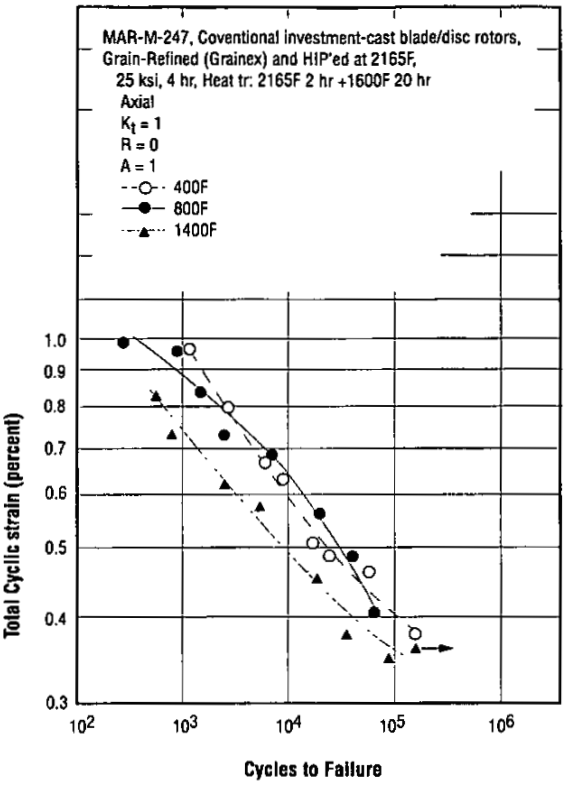

Figure 3.5.2.4 Low-cycle fatigue life at three elevated temperatures as a function of total cyclic strain for investment-cast, grain-refined HIP'ed alloy (Ref. 25)

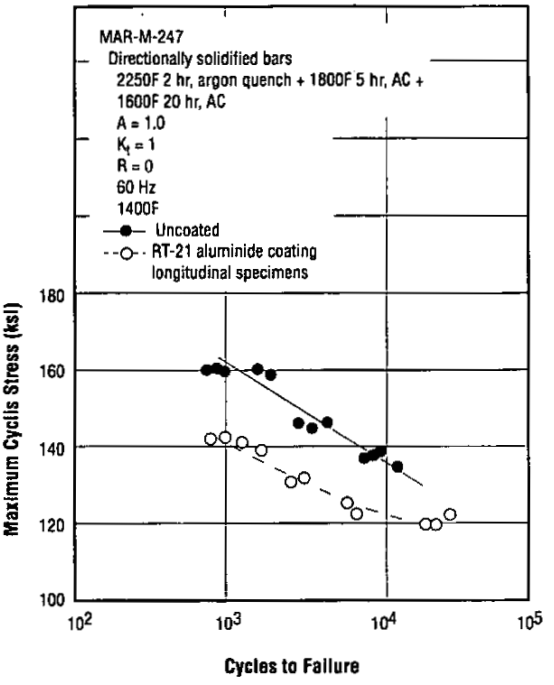

Figure 3.5.2.5 Low-cycle fatigue life under load control at 1400F for smooth coated and uncoated specimens from directionally solidified test bars (Ref. 2)

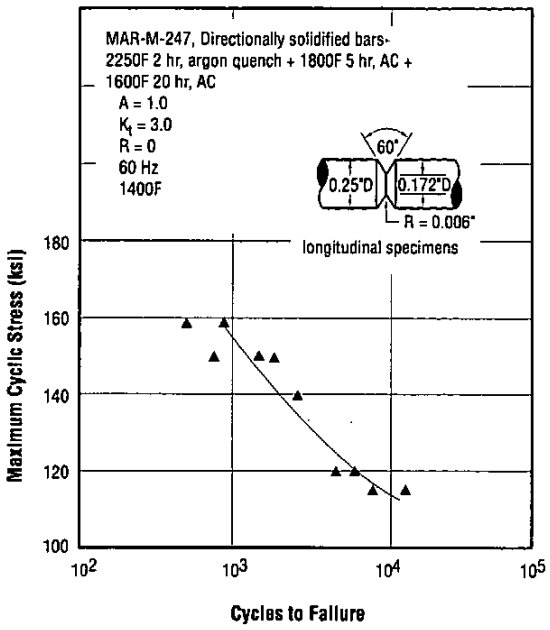

Figure 3.5.2.6 Low-cycle fatigue under load control at 1400F for notched uncoated specimens from directionally solidified test bars (Ref. 2)

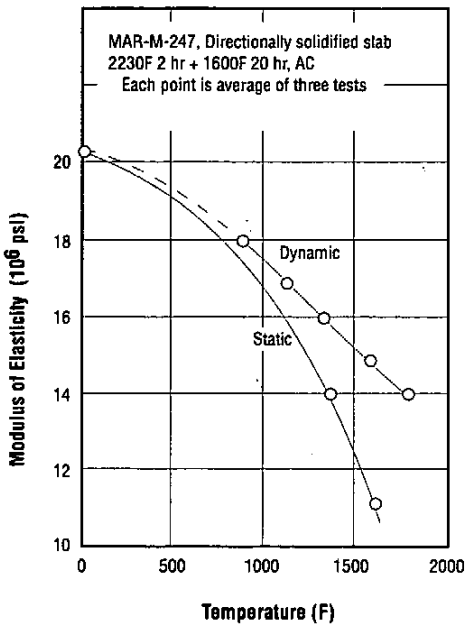

Figure 3.6.2.2.1 Modulus of elasticity in longitudinal [001] grain orientation for test specimens machined from directionally solidified alloy (Ref. 2)

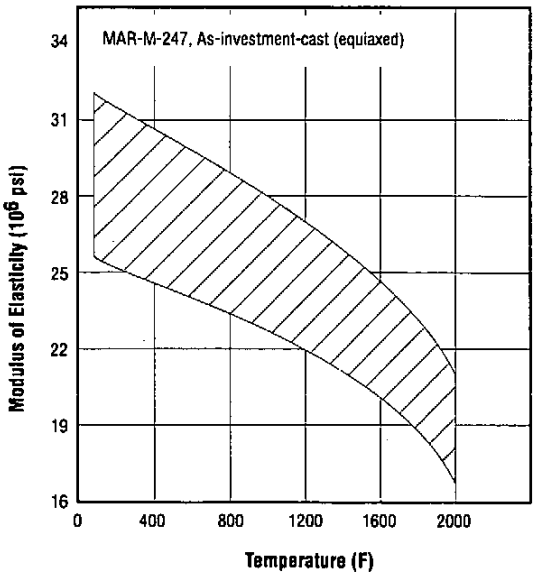

Figure 3.6.2.3 Range of modulus-of-elasticity values determined by numereous tests on equiaxed castings at temperatures from 75F to 2000F (Ref. 32)

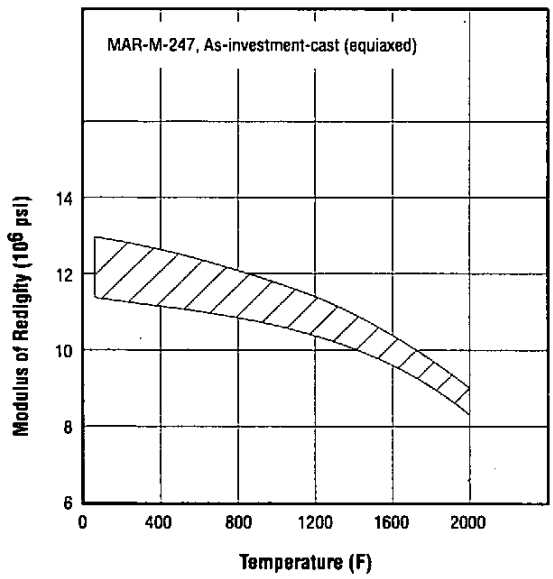

Figure 3.6.3.1 Range of modulus-of-rigidity values determined by numereous tests on equiaxed castings at temperatures from 75F to 2000F (Ref. 32)